Environmental Science
Water Research & Technology

Accepted Manuscript

ROYAL SOCIETY OF CHEMISTRY

rsc.li/es-water

Water Impact Statement

Membrane fouling and subsequent wetting hinders water production and quality in membrane distillation (MD). Real feed streams always contain varying foulants, including colloidal and organic foulants, which potentially leads to combined fouling. An in-depth understanding of the foulant-foulant, and foulant-membrane interactions can shed light on the fouling mechanisms during MD filtration and guide corresponding pre-treatment approaches to minimize MD fouling.

Synergistic effect of combined colloidal and organic fouling in membrane distillation: measurements and mechanisms

Environmental Science: Water Research & Technology

Revised: 10 July 2016

Wenli Qin [1,2,3], Jianhua Zhang [1], Zongli Xie [2*], Derick Ng[2], Ying Ye [3], Stephen R. Gray [1], Ming Xie [1*]

[1] Institute for Sustainability and Innovation, College of Engineering and Science, Victoria University, Melbourne, VIC 8001, Australia

[2] CSIRO Manufacturing, private bag 10, Clayton South MDC, VIC 3169, Australia

[3] Institute of Marine Geology and Resource, Ocean College, Zhejiang University, Zhoushan, Zhejiang 316021, China

[*] Corresponding authors: ming.xie@vu.edu.au; Ph: +61 (3) 9919 8174; zongli.xie@csiro.au, Ph: +61 (3) 9545 2938.

Abstract

We examined the synergistic effect of combined fouling in MD process with three organic foulants – alginate, bovine serum albumin (BSA), and humic acid – in the presence of colloidal silica particles. Membrane fouling profiles were quantified by water flux decline and permeate conductivity. Mechanisms of the synergistic effect of combined fouling were revealed by light scattering measurements and inferred spectra of foulant-foulant interaction and foulant-membrane interaction. Membrane fouling morphology and element mapping provided further details of transport of colloidal silica particles and elucidated the mechanisms for silica-induced pore wetting. Specially, gelation of alginate formed an alginate layer on membrane surface and prevented penetration of silica particles into membrane matrix, which was confirmed by silicon element mapping as well as IR spectra. Adsorption of BSA protein by colloidal silica aggregates led to a sharp water flux decline and a partial pore wetting. Humic acid, forming a coil structure in high salinity, exhibited limited interaction with colloidal silica that penetrated into the membrane matrix and wetted membrane pores, thereby compromising the product water quality. Results showed that the combined organic fouling with colloidal silica particle not only deteriorated water production, but also compromised product quality by partial membrane wetting.

1. Introduction

Membrane distillation (MD), a thermally-driven membrane process, holds the promise in brine management. The discontinuous nature of water transport through porous, hydrophobic membrane in MD process ensures that the water production is largely independent of the feed solution salinity. In addition, MD can offer complete rejection of all non-volatile constituents, such as ions, dissolved non-volatile organics, colloids, and pathogenic agents, in the feed solution. MD process can be operated in four different configurations including vacuum, air gap, sweep gas, and direct contact membrane distillation (DCMD) [1]. In particular, the DCMD configuration is well suited for brine treatment and concentration valuable products, where water is the main distillate product. As a result, the MD process was proposed to treat a wide range of challenging saline waste streams, such as reverse osmosis (RO) brine [2-5], coal seam gas brine [6-8], drilling fluids from oil and gas exploration [9, 10], sludge centrate [11-14], and diary streams [15, 16]. For instance, MD was demonstrated to be a feasible and effective process capable of consistently producing high quality distillate (conductivity less than 10 μS/cm) from high salinity brines (70,000 mg/L total dissolved solids) in a desalination plant. MD process was also capable of achieving high water recovery (more than 85%) from coal seam gas brine [6], and high ammonia concentration (at least four-fold) from pig manure [17].

Despite the effectiveness and robustness of MD filtration, membrane fouling, even wetting, can be detrimental to the MD operation [18, 19], which decreases the driving force for permeation and demands frequent interruptions to operating systems for membrane cleaning [20, 21]. For instance, organic fouling consisting mainly of proteins, lipids and carbohydrates, was found to cause severe membrane fouling and reduced ammonia recovery from manure streams [17]. Efforts were made to quantify and elucidate the mechanisms during MD fouling [22]. Previous studies suggested that the deposition of various foulants onto the membrane surface not only reduced the vapour pressure difference through the membrane, but also changed the hydrophilicity of membrane surface, thereby initiating pore wetting and compromising product water quality [23-25]. Consequently, strategies to control MD fouling were proposed, including pre-treatments and advanced membrane surface modification for antifouling [20]. Specifically, microfiltration or ultrafiltration was adopted to remove particulates matters and macromolecular compounds, prior to the MD process. For instance, one step of microfiltration before MD process could improve permeate flux by 25% [26]; and an ultrafiltration pre-treatment for MD process resulted in oil concentration less than 5 mg/L [27].

On the other hand, modification and fabrication MD membrane can also imparts membrane anti-fouling property and mitigates deleterious membrane fouling and wetting, thereby improving the nutrient recovery efficiency of MD in processing challenging saline waste streams [28-30]. For example, Razmjou et al. [31] fabricated a superhydrophobic polyvinylidene fluoride (PVDF) MD membrane with TiO_2 nanoparticles providing hierarchical structures with multilevel roughness on the membrane surface. The resultant MD membrane demonstrated a much higher water flux recovery after humic acid fouling in comparison to the pristine PVDF membrane.

The ability of MD process to treat challenging saline waste streams with complex mixture of varying foulants relied on an in-depth understanding the synergistic interaction of combined foulants. For example, the synergistic interaction between organic foulants and colloidal silica, as well as the foulant-membrane interaction during MD process remained largely unknown. Understanding the synergistic effect of combined fouling is critical to assess and management MD process in treating challenging waste streams. One important conclusion from previous investigations of combined fouling in RO process was that combination of inorganic colloids and organic foulants significantly enhanced fouling, which was more than the sum of the individual effects from organic macromolecules and inorganic colloids [32-34]. However, it was uncertain whether this is true in MD process because of the difference of driving force (pressure driven in RO vs vapour driven in MD) as well as operating condition (e.g., much higher feed temperature in MD). In addition, MD membrane was microporous; by contrast RO membrane was dense nanoporous. The discrepancy of pore size can also affect the transport of foulants with relatively small size in MD, such as colloidal silica particle. The deposition and subsequent transport of colloidal silica through MD membrane can be altered due to the presence of other organic foulants, thereby increasing the uncertainty of the fouling profile as well as complicating fouling mechanisms.

In this study, we examined the combined fouling in MD process induced by silica colloidal particle with varying organic foulants. Water flux decline and permeate water quality were compared between individual foulant and combined foulants in MD filtration. Synergistic effect of combined fouling was investigated by exploring foulant-foulant interaction with light scattering and foulant-membrane interaction by Fourier transform infrared spectroscopy. Transport and distribution of colloidal silica particle during the MD fouling was captured by elemental mapping of the cross section of the fouled membrane, thereby elucidating the synergistic fouling mechanisms of combined foulants in MD process.

2. Materials and Methods

2.1 Membrane and model foulants

A hydrophobic, microporous membrane from Porous Membrane Technology (Ningbo, China) was used for the MD filtration. The MD membrane consists of a thin polytetrafluoroethylene (PTFE) active layer on top of a polypropylene (PP) support layer. The pore size and porosity of the membrane were 0.5 μm and 70%, respectively. The membrane thickness was 120 μm, of which the active layer was approximately 10 μm.

Both colloidal and organic foulants were used in the MD process. Ludox HS-30 silica colloids from Sigma-Aldrich were used to represent colloidal foulant, while humic acid, alginate and bovine serum albumin (BSA) were used to simulate organic foulants. A stock solution (5 g/L) with each organic foulant was prepared by dissolving each organic foulant into Milli-Q water and stored in a sterilized amber glass bottle at 4 °C. The Ludox HS-30 colloidal silica suspension (35 wt%) was sonicated for 10 min to ensure complete dispersion before adding to the feed solution.

2.2 Membrane distillation apparatus

Direct contact MD (DCMD) experiments were conducted using a closed-loop bench-scale membrane test apparatus (Figure S1, Electron Supplementary Information). The membrane cell was made of acrylic plastic to minimize heat loss to the surroundings. The flow channels were engraved in each of two acrylic blocks that made up the feed and permeate semi-cells. Each channel was 0.3 cm deep, 9.5 cm wide, and 14.5 cm long; and the total active membrane area was 138 cm^2.

Temperatures of feed and distillate solutions were controlled by two heater/chillers (Polyscience, IL, USA), and were continuously recorded by temperature sensors that were inserted at the inlet and outlet of the membrane cell. Both feed and distillate streams were co-currently circulated by two gear pumps. The same crossflow rate of 600 mL min^{-1} was applied to both feed and distillate co-currently in order to minimize the pressure difference across the MD membrane. Weight change of the distillate tank was recorded by an electronic balance (Mettler Toledo, OH, USA) with a data logger. All piping used in the DCMD test unit was covered with insulation foam to minimize heat loss.

2.3 Experimental protocol

MD fouling experiments were conducted using individual foulant as well as a solution of combined foulants. Specifically, each foulant (i.e., silica colloidal particle, humic acid, alginate and BSA) of 50 mg/L was added into 1 M NaCl feed to examine the MD fouling; the synergistic effect was investigated by adding varying organic foulants with silica colloidal particle into 1 M NaCl solution, denoted as silica with humic acid, silica with alginate, and silica with BSA, respectively.

Feed and distillate volumes of four and one litre were used, respectively. Temperate of inlet feed solution was 50 ºC; while that of the distillate inlet stream was 20 ºC in all experiments. A new membrane sample was used for each experiment. Conductivity of the distillate was measured by a conductivity meter (HQ14d, Hach, CO) every 30 minutes. The MD filtration experiment was terminated when water flux decline was beyond 50% of the initial water flux, corresponding to attainment of approximately 1,500 mL permeate. At the conclusion of each experiment, the membrane was removed from the membrane cell and was kept in a desiccator for subsequent characterisation.

2.4 Analytic techniques

2.4.1 Feed solution characterisation

Change of particle size and zeta potential of feed solution were analysed by a zetasizer (Zetasizer Nano ZSP, Malvern, UK). Specifically, evolution of foulant size and feed solution zeta potential were measured by dynamic light scattering and laser Doppler microelectrophoresis, respectively. These analyses indicated the foulant-foulant interaction during the MD fouling.

2.4.2 Key membrane properties

Key membrane properties were measured at the completion of MD fouling experiment, including contact angle by dynamic contact angle analyser (FTA200, VA) and pore size distribution by a capillary flow porometer (POROMETER 3G, Quantachrome Instrument, FL).

Chemical composition of the fouling layer at specific time intervals was evaluated by Attenuated total reflection Fourier transform infrared (ATR-FTIR) spectrometer (Thermo Scientific Nicolet 6700) equipped with an ATR accessory consisting of a ZnSe plate (45° angle of incidence). Absorbance spectra were measured with 64 scans of each sample at a spectral resolution of 2 cm^{-1}. Background measurements in air were collected before each

membrane sample measurement. ATR-FTIR spectra were collected at two different spots for each membrane sample.

2.4.3 Fouling layer imaging

Morphology of the fouling layer deposited onto the membrane surface was examined by a scanning electron microscope (SEM, Merlin ZIESS GEMINI2). Both membrane surface and cross section were imaged. The membrane samples were dried in a desiccator, and were cracked in liquid nitrogen to create the cross section. Extreme care was taken when preparing the fouled membrane samples to ensure that the fouling layer remained intact. Distribution of key elements – carbon (C), oxygen (O), fluorine (F), silicon (Si) – in the fouled membrane cross section was mapped by energy-dispersive X-ray spectroscopy (EDS).

3. Results and discussion

3.1 Fouling behaviours

3.1.1 Individual foulant

Marked differences were observed between organic fouling (i.e., alginate, humic acid and BSA) and silica colloidal fouling in terms of water flux decline and permeate water quality (Figure 1). Generally, all three organic foulants resulted in a moderate water flux decline as well as a continuous decrease of permeate conductivity (Figures 1A-C). A close examination of the organic fouling profile showed that humic acid and BSA (Figures 1B-C) led to a more severe water flux decline in comparison with alginate (Figure 1A), which possessed a hydrophilic nature. BSA, initiating hydrophobic association with the MD membrane, resulted in more than 50% water flux decline (Figure 1B). However, all three organic foulants did not exhibit membrane wetting during filtration, which would have been detected by an increase of permeate conductivity. Indeed, previous studies also reported that organic fouling in MD process did not lead to membrane wetting [15, 16].

Unlike organic foulants, colloidal silica induced a severe water flux decline from 36 to 6 $Lm^{-2}h^{-1}$ at the cumulative permeate volume of 1,000 mL (Figure 1D); and concomitantly, a sharp increase in permeate conductivity indicated the undesirable wetting of the hydrophobic MD membrane, thereby compromising the product water quality. Such significant water flux decline was mainly driven by the deposition and aggregation of foulants onto membrane surface, rather than the concertation of feed NaCl solution that only

194 led to marginal decrease in water vapour pressure difference through the membrane. Due to
195 the much smaller silica particle size than the MD membrane pore size, penetration of
196 colloidal silica into the membrane pore first initiated pore wetting and intrusion [35], followed
197 by internal pore blockage, thereby leading to severe water flux decline as well as
198 deterioration of product water quality. Such detrimental membrane wetting was also evident
199 by the significantly lower contact angle of colloidal silica fouled membrane (20 ± 2 ºC) in
200 comparison with that of alginate (81.9 ± 1.2 ºC), humic acid (79.6 ± 2.2 ºC) or BSA (78.6 ±
201 2.8 ºC) fouled membranes (Figure S2, Electronic Supplementary Information). The MD
202 membrane became hydrophilic after fouling with colloidal silica particle and presented a
203 reduced liquid entry pressure, thereby enabling the transport of salt from feed to distillate
204 stream through the membrane.

205 The ability of penetrating into and wetting of the MD membrane by the colloidal
206 silica may significantly alter the fouling behaviour of combined foulants (colloidal silica with
207 organic foulants), and warranted a closer examination on the fouling profile and the
208 underlying mechanisms.

209 **[Figure 1]**

210 *3.1.2 Combined silica colloidal and organic foulants*

211 In general, combined fouling in MD process exhibited more severe water flux decline
212 and changes in product water quality in comparison with individual foulants. A reduction in
213 average pore size (Figure S3, Electronic Supplementary Information) as well as the
214 membrane surface hydrophobicity (Figure S2, Electronic Supplementary Information)
215 resulted from the various fouling layers.

216 *(a) Colloidal silica with alginate*

217 Colloidal silica with alginate induced a severe water flux decline in comparison with
218 alginate only (Figure 1A). The water production was compromised, attaining only 800 mL
219 permeate when more than 50% water flux decline was reached (Figure 2A). However, no salt
220 passage through the membrane (i.e., membrane wetting) was observed, which was evident by
221 a continuous decrease in permeate conductivity.

222 Fouling layer morphology demonstrated a cake layer that compromised alginate gel
223 with clusters of colloidal aggregates (Figures 2B and C). It is hypothesized that the gelation
224 of viscous alginate formed a cage-like structure [36] that can capture and trap colloidal silica,
225 thereby minimizing the penetration of silica into membrane matrix as well as pore wetting.

[Figure 2]

(b) Colloidal silica with BSA

Sharp water flux decline was demonstrated during the filtration of BSA with colloidal silica. Water flux decreased from 50 to 8 $Lm^{-2}h^{-1}$ within production of only 500 mL distillate (Figure 3A), which was one third production of filtering pure BSA (Figure 1B). More alarming, a small but discernible increase in permeate conductivity was observed at the conclusion of the fouling, indicating the occurrence of partial pore wetting.

The cake layer induced by BSA with silica colloidal was distinctive in terms of stack of globular BSA protein macromolecular with size of 1 μm with silica aggregates (Figures 3B and C). The size of BSA protein with silica aggregates was twice as large as the MD membrane pore and resulted in a severe pore blockage, thereby leading to dramatic water flux decline. BSA proteins tend to absorbed onto the surface of colloidal silica, and aggregated into large particles. Previous studies also showed that BSA protein was adsorbed by colloidal silica [33, 37], which was evident by an increase of zeta potential from -10.3 to -5.7 mV between BSA protein and colloidal particle (Figure S4, Electronic Supplementary Information). As a result, it is hypothesized that the silica – BSA interaction led to a significant increase in particle size via adsorption, and blocked MD membrane pore, resulting in a severe loss in water production.

[Figure 3]

(c) Colloidal silica with humic acid

Water flux decline during processing feed with colloidal silica and humic acid was similar to that by colloidal silica with alginate. Only 800 mL permeate was collected when approximate 50% water flux decline was achieved (Figure 4A). However, a significant increase in permeate conductivity suggested detrimental membrane wetting (Figure 4A). Humic acid became a compact coil under high ionic strength, and had negligible adsorption with colloidal silica [38], which was evident by the largely unchanged zeta potential (Figure S2, Electronic Supplementary Information). As a result, it is hypothesized that humic acid and colloidal silica deposited onto membrane surface independently and formed the cake layer. Indeed, the fouling layer morphology showed the coiled humic acid was layered on top of colloidal silica (Figures 4B and C). The colloidal silica cake layer adjacent to the membrane surface may partially wet the membrane pore, and enable the penetration of silica particles into the membrane matrix, thereby resulting in membrane wetting.

[Figure 4]

4. Quantifying synergistic fouling mechanisms

4.1 Colloidal silica – organic foulant interaction

We employed dynamic light scattering to track the change in foulant particle size during the MD fouling, and Fourier transform infrared (FTIR) spectroscopy to examine the chemical information at the membrane interface in a time-resolved manner. This information can index and capture the sequence of fouling layer development.

Colloidal silica-organic foulant interaction in the feed solution was quantified by the changes of particle size (Figure 5). Specifically, two clear peaks at 21 nm and 396 nm represented silica and alginate, respectively, at the beginning of filtration (Figure 5A). The increase of intensity as well as particle size to 955 nm indicated the gelation of alginate from the cumulative permeate volume 200 mL to the completion of filtration. The BSA-colloidal silica interaction resulted in a swift particle size growth from 400 nm to 1.5 μm, which was consistent with the severe water flux decline due to the pore blockage (Figure 5B). Humic acid and colloidal silica showed distinctive peaks as particle size increased as filtration progressed (Figure 5C), which indicated a relatively mild interaction and was consistent with less severe water flux decline.

[Figure 5]

The FTIR spectra shed light on the deposition sequence of the foulants onto the membrane surface. For instance, as filtration progressed, the major peak increase was at wavenumber of 1634 cm^{-1} (C=O stretching) [39, 40], indicating the presence of alginate on the membrane surface (Figure 6A). This observation was consistent with the hypothesis that alginate formed the cage-like structure and the alginate gel layers blocked the membrane pore during the fouling. In the case of colloidal silica with BSA, the increase at the wavenumbers of 1642 cm^{-1} (C=O stretching), and 1055 cm^{-1} (Si=O stretching) suggested the presence of protein as well as the silica on the membrane surface (Figure 6B). This chemical information agreed with the change in particle size, both of which demonstrated that the adsorption between colloidal silica and BSA led to an aggregate with particle size over 1 μm, thereby resulting severe water flux decline. The deposition of colloidal silica was earlier than that of humic acid onto the membrane because the occurrence of Si=O bond at wavenumber 1055

289 cm^{-1} (at cumulative permeate volume of 500 mL) was prior to the appearance of C=O bond at
290 wavenumber of 1642 cm^{-1} (at cumulative permeate volume of 800 mL) (Figure 6C). The
291 progress of FTIR spectra was consistent with the particle size growth, as well as the
292 hypothesis that limited interaction occurred between humic acid and colloidal silica during
293 the filtration.

294 **[Figure 6]**

295 *4.2 Transport of colloidal silica into membrane pore*

296 Membrane pore wetting and subsequent deterioration of product water was observed
297 using combined foulants. The transport and penetration of colloidal particle through the
298 membrane matrix can be the culprit for membrane wetting. We imaged and mapped the key
299 elements of membrane cross section to demonstrate the spatial distribution of colloidal silica
300 particle. The fluorine layer represented the active layer of the MD membrane, which was
301 made of polytetrafluoroethylene. The oxygen and carbon elements enable the visualization of
302 organic foulants. With these benchmarks, we can determine the location of silica in the
303 fouling layer, and possible penetration of silica into the membrane.

304 A close examination of the silicon element shed light on the mechanism of membrane
305 wetting (Figure 7). For instance, the fouling layer of colloidal silica with alginate showed a
306 compact and continuous layer of silicon (Figure 7A), without penetrating through the fluorine
307 layer, which suggested the majority of colloidal silica was rejected by the membrane. This
308 result agreed well with the continuous decrease in permeate conductivity and further
309 confirmed the hypothesis that the colloidal silica was trapped by the alginate gel, thereby
310 blocking the membrane pore and inducing severe water flux decline.

311 In the case of colloidal silica with BSA, the silicon element mapping was aggravated
312 by the BSA protein, resulting in a thick silicon element layer (Figure 7B). More importantly,
313 the silicon layer partially overlapped with the fluorine layer, which indicated the penetration
314 of silica colloidal particles into the membrane matrix. Similar, yet more severe silica
315 penetration was observed in the case of colloidal silica with humic acid (Figure 7C). The
316 silicon element exhibited strong presence within membrane active layer, with some silica
317 colloidal particles penetrating into the membrane. This observation indicated membrane
318 wetting and agreed well with the significant increase in permeate conductivity. In addition,
319 this element mapping further confirmed the hypothesis that the negligible interaction between

colloidal silica and humic acid resulted in a layered structure with colloidal silica particles being deposited first onto the membrane, thereby facilitating pore wetting during the fouling.

[Figure 7]

Based on the aforementioned experimental observation, we can conceptually picture the fouling mechanisms of colloidal silica particle with varying organic foulants. Different mechanisms were presented in the combined fouling: (a) colloidal silica particles were trapped and caged by the gelation of alginate, thereby leading to a gel layer onto the membrane surface. Such interaction resulted in severe water flux decline, but did not compromise the product water quality because minimum penetration of silica into membrane matrix; (b) colloidal silica particle adsorbed hydrophobic BSA protein, and resulted in a significant increase in particle size beyond 1 μm. Such aggregates partially blocked the membranes, and led to a swift water flux decline. Unbound silica particles also partially interacted with membrane surface, and resulted in a mild pore wetting; (c) humic acid, being coil structure in high salinity, showed limited interaction with colloidal silica particles. As a result, the colloidal silica particles penetrated into the membrane matrix and wetted membrane pores, thereby compromising the product water quality.

4.3 Implications

Markedly different response of combined fouling with colloidal silica and varying organic foulants had significant implication in the management of MD process in treating waste streams with high fouling propensity. The interplay of colloidal silica particle with organic foulants during the filtration profoundly altered the MD performance and product water quality. The ability of colloidal silica particles to wet pores also provided guidance in the pre-treatment of feed streams, particularly the removal of particulate foulants prior to MD process, in order to minimize membrane wetting, thereby maintaining the robustness and sustainability of the MD process.

5. Conclusion

We examined the mechanisms of synergistic effect of MD membrane fouling induced by three organic foulants – alginate, BSA and humic acid – in the presence of colloidal silica particles. Significantly different fouling profiles were observed in terms of water flux decline and product water quality. All combined fouling exhibited more severe water flux decline in comparison with fouling by individual organic foulant. Gelation of alginate formed an alginate layer on membrane surface and prevented penetration of silica particles into membrane matrix, which was confirmed by silicon element mapping as well as IR spectra. Adsorption of BSA protein by colloidal silica aggregates led to a sharp water flux decline and a partial pore wetting. Humic acid, forming a coil structure in high salinity, exhibited limited interaction with colloidal silica and colloidal silica penetrated into the membrane and leading to membrane pore wetting, thereby compromising the product water quality.

6. Acknowledgments

The authors would like to acknowledge the CSIRO Manufacturing for the financial support of this work. W. Qin would like to thank the scholarship from Zhejiang University via Doctoral Student Exchange Program. M. Xie thanked the award of Vice Chancellor Early Career Researcher Fellowship from Victoria University. A/Prof. Xiaosheng Ji from Zhejiang University is greatly acknowledged for the helpful discussion. Ms Lee Russell and Mr Mark Greaves from CSIRO Manufacturing are greatly acknowledged from their help on membrane characterisation work.

7. References

1. A. Alkhudhiri, N. Darwish and N. Hilal, *Desalination*, 2012, **287**, 2-18.
2. S. Adham, A. Hussain, J. M. Matar, R. Dores and A. Janson, *Desalination*, 2013, **314**, 101-108.
3. X. Ji, E. Curcio, S. Al Obaidani, G. Di Profio, E. Fontananova and E. Drioli, *Separation and Purification Technology*, 2009, **71**, 76-82.
4. L. Mariah, C. A. Buckley, C. J. Brouckaert, E. Curcio, E. Drioli, D. Jaganyi and D. Ramjugernath, *Journal of Membrane Science*, 2006, **280**, 937.
5. C. R. Martinetti, A. E. Childress and T. Y. Cath, *Journal of Membrane Science*, 2009, **331**, 31-39.
6. H. C. Duong, A. R. Chivas, B. Nelemans, M. Duke, S. Gray, T. Y. Cath and L. D. Nghiem, *Desalination*, 2015, **366**, 121-129.
7. H. C. Duong, S. Gray, M. Duke, T. Y. Cath and L. D. Nghiem, *Journal of Membrane Science*, 2015, **493**, 673-682.
8. A. Alkhudhiri, N. Darwish and N. Hilal, *Desalination*, 2013, **309**, 46-51.
9. X.-M. Li, B. Zhao, Z. Wang, M. Xie, J. Song, L. D. Nghiem, T. He, C. Yang, C. Li and G. Chen, *Water Science and Technology*, 2014, **69**, 1036-1044.
10. D. L. Shaffer, L. H. Arias Chavez, M. Ben-Sasson, S. Romero-Vargas Castrillón, N. Y. Yip and M. Elimelech, *Environmental Science & Technology*, 2013, **47**, 9569-9583.
11. T. Y. Cath, D. Adams and A. E. Childress, *Journal of Membrane Science*, 2005, **257**, 111-119.
12. J. Phattaranawik, A. G. Fane, A. C. S. Pasquier and W. Bing, *Desalination*, 2008, **223**, 386-395.
13. M. Xie, L. D. Nghiem, W. E. Price and M. Elimelech, *Environmental Science & Technology*, 2013, **47**, 13486-13493.
14. M. Xie, L. D. Nghiem, W. E. Price and M. Elimelech, *Environmental Science & Technology Letters*, 2014, **1**, 191-195.
15. A. Hausmann, P. Sanciolo, T. Vasiljevic, M. Weeks, K. Schroën, S. Gray and M. Duke, *Journal of Membrane Science*, 2013, **442**, 149-159.
16. A. Hausmann, P. Sanciolo, T. Vasiljevic, M. Weeks, K. Schroën, S. Gray and M. Duke, *Journal of Membrane Science*, 2013, **441**, 102-111.

17. A. Zarebska, Á. C. Amor, K. Ciurkot, H. Karring, O. Thygesen, T. P. Andersen, M.-B. Hägg, K. V. Christensen and B. Norddahl, *Journal of Membrane Science*, 2015, **484**, 119-132.
18. Z. Wang, M. Elimelech and S. Lin, *Environmental Science & Technology*, 2016, **50**, 2132-2150.
19. Z. Wang, D. Hou and S. Lin, *Environmental Science & Technology*, 2016, **50**, 3866-3874.
20. L. D. Tijing, Y. C. Woo, J.-S. Choi, S. Lee, S.-H. Kim and H. K. Shon, *Journal of Membrane Science*, 2015, **475**, 215-244.
21. D. M. Warsinger, J. Swaminathan, E. Guillen-Burrieza, H. A. Arafat and J. H. Lienhard V, *Desalination*, 2015, **356**, 294-313.
22. M. Xie, H. K. Shon, S. R. Gray and M. Elimelech, *Water Research*, 2016, **89**, 210-221.
23. J. W. Chew, W. B. Krantz and A. G. Fane, *Journal of Membrane Science*, 2014, **456**, 66-76.
24. G. Naidu, S. Jeong, S.-J. Kim, I. S. Kim and S. Vigneswaran, *Desalination*, 2014, **347**, 230-239.
25. Y. Z. Tan, J. W. Chew and W. B. Krantz, *Journal of Membrane Science*, 2016, **504**, 263-273.
26. A. M. Alklaibi and N. Lior, *Desalination*, 2005, **171**, 111-131.
27. M. Gryta, K. Karakulski and A. W. Morawski, *Water Research*, 2001, **35**, 3665-3669.
28. S. Lin, S. Nejati, C. Boo, Y. Hu, C. O. Osuji and M. Elimelech, *Environmental Science & Technology Letters*, 2014, **1**, 443-447.
29. Y. Liao, R. Wang and A. G. Fane, *Journal of Membrane Science*, 2013, **440**, 77-87.
30. Y. Liao, R. Wang and A. G. Fane, *Environmental Science & Technology*, 2014, **48**, 6335-6341.
31. A. Razmjou, E. Arifin, G. Dong, J. Mansouri and V. Chen, *Journal of Membrane Science*, 2012, **415–416**, 850-863.
32. M. Schulz, A. Soltani, X. Zheng and M. Ernst, *Journal of Membrane Science*, 2016, **507**, 154-164.
33. Q. Li and M. Elimelech, *Journal of Membrane Science*, 2006, **278**, 72-82.
34. A. E. Contreras, A. Kim and Q. Li, *Journal of Membrane Science*, 2009, **327**, 87-95.
35. J. Gilron, Y. Ladizansky and E. Korin, *Industrial & Engineering Chemistry Research*, 2013, **52**, 10521-10529.
36. H. Hecht and S. Srebnik, *Biomacromolecules*, 2016, **17**, 2160-2167.

37. M. Wiśniewska, K. Szewczuk-Karpisz and D. Sternik, *Journal of Thermal Analysis and Calorimetry*, 2015, **120**, 1355-1364.
38. C. Y. Tang, Y.-N. Kwon and J. O. Leckie, *Environmental Science & Technology*, 2007, **41**, 942-949.
39. M. Xie, C. Y. Tang and S. R. Gray, *Desalination*, 2016, **392**, 85-90.
40. M. Xie and S. R. Gray, *Journal of Membrane Science*, 2016, **513**, 250-259.

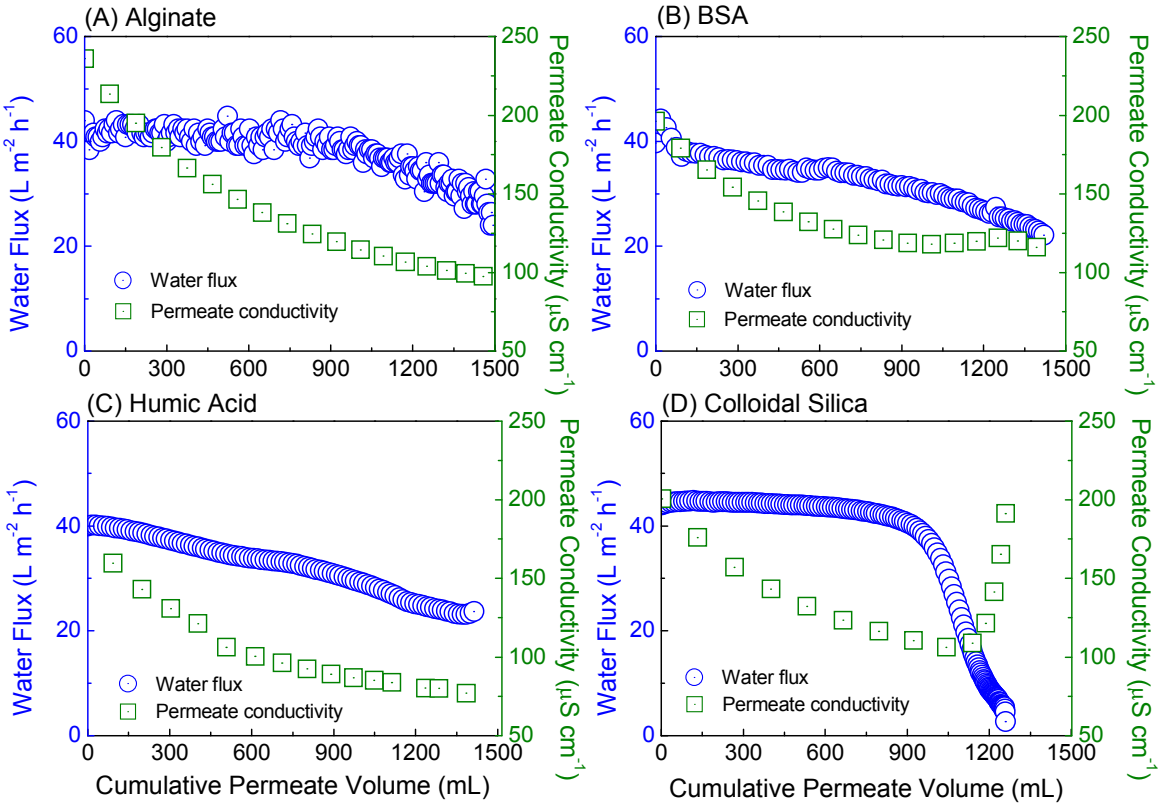

Figure 1: Water flux and permeate conductivity as a function of cumulative permeate volume during membrane distillation fouling using (A) alginate, (B) BSA, (C) humic acid and (D) colloidal silica. Experimental conditions were feed solution contained 1 M NaCl with concentrations of individual alginate, BSA, humic acid and colloidal silica as 100 mg/L, 100 mg/L, 100 mg/L, and 500 mg/L, respectively. Distillate solution was tap water. Temperatures of feed and distillation were 50ºC and 20 ºC, respectively. Crossflow rate for feed and distillate was 600 mL/min co-currently.

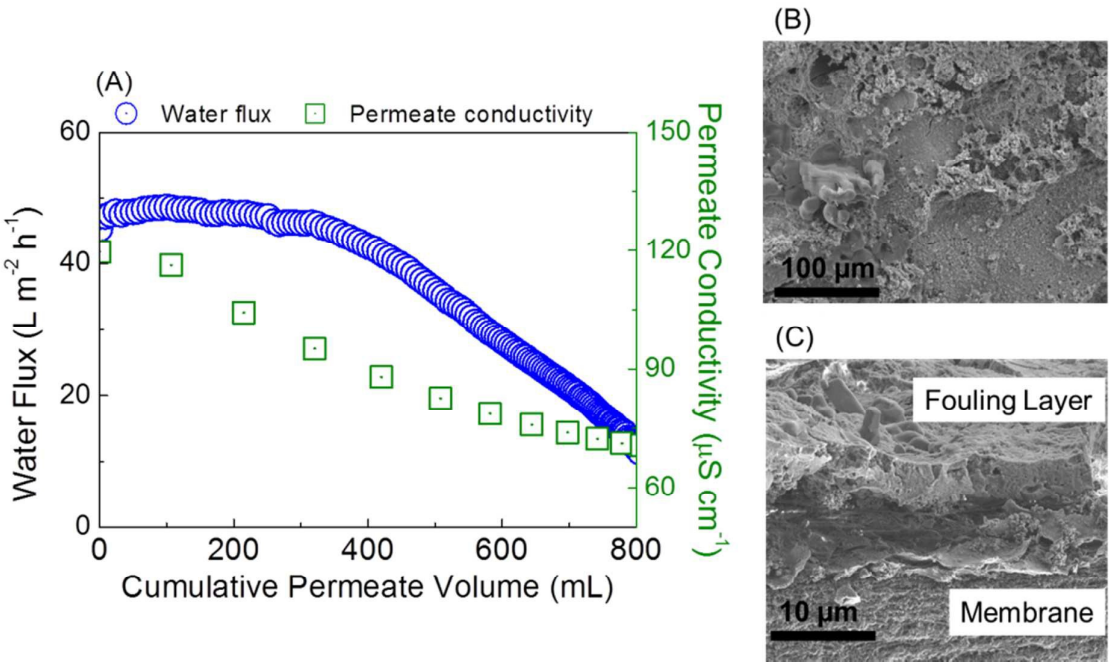

Figure 2: Membrane distillation fouling profile by colloidal silica with alginate: (A) water flux and permeate conductivity as a function of cumulative permeate volume; and micrographs of fouled membrane (B) surface and (C) cross section. Experimental conditions were feed solution contained 1 M NaCl with concentrations of 100 mg/L alginate, and 500 mg/L colloidal silica. Distillate solution was tap water. Inlet temperatures of feed and distillate were 50 ºC and 20 ºC, respectively. Crossflow rate for feed and distillate was 600 mL/min co-currently.

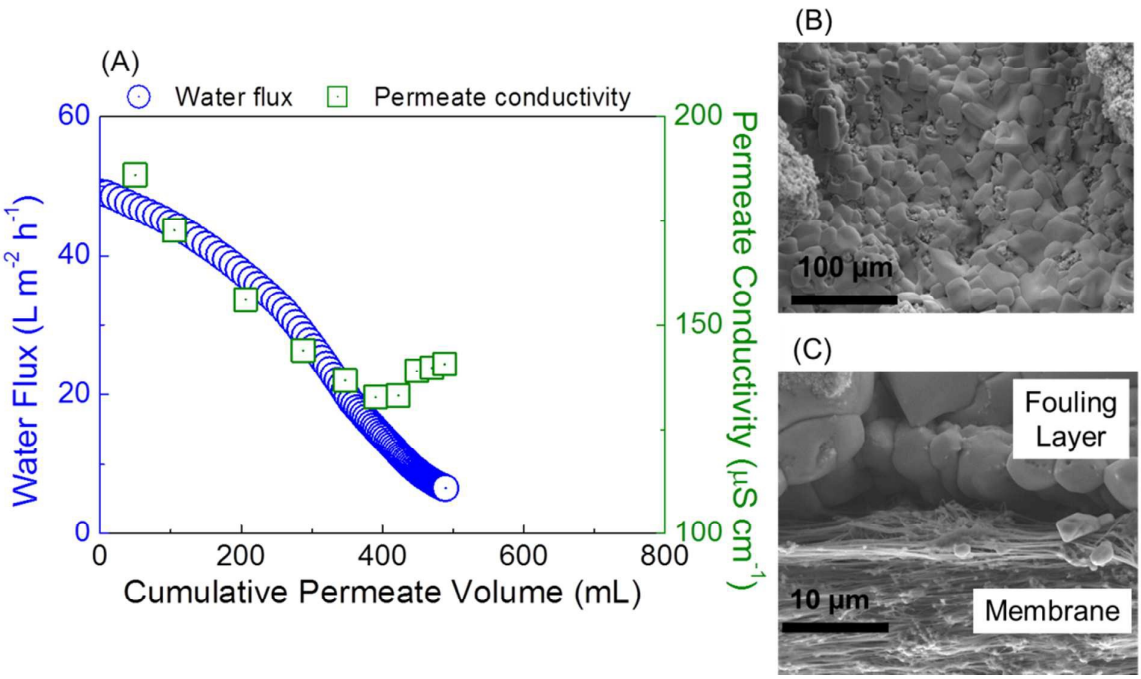

Figure 3: Membrane distillation fouling profile by colloidal silica with BSA: (A) water flux and permeate conductivity as a function of cumulative permeate volume; and micrographs of fouled membrane (B) surface and (C) cross section. Experimental conditions were feed solution contained 1 M NaCl with concentrations of 100 mg/L BSA, and 500 mg/L colloidal silica. Distillate solution was tap water. Inlet temperatures of feed and distillation were 50ºC and 20 ºC, respectively. Crossflow rate for feed and distillate was 600 mL/min co-currently.

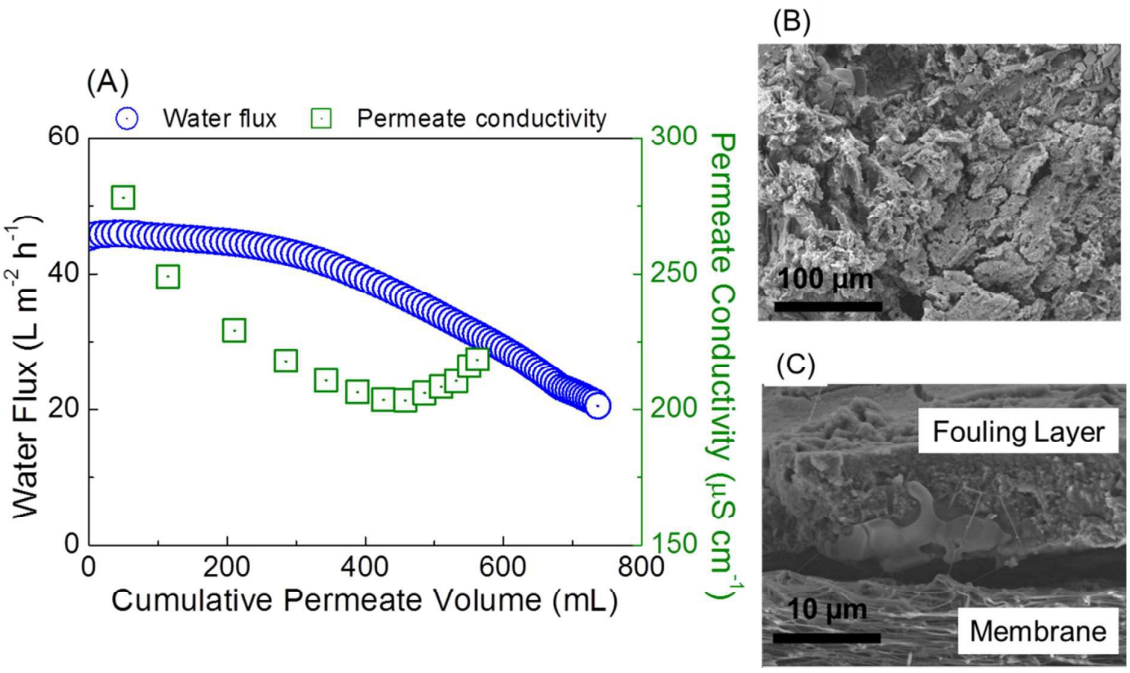

Figure 4: Membrane distillation fouling profile by colloidal silica with humic acid: (A) water flux and permeate conductivity as a function of cumulative permeate volume; and micrographs of fouled membrane (B) surface and (C) cross section. Experimental conditions were feed solution contained 1 M NaCl with concentrations of 100 mg/L humic acid, and 500 mg/L colloidal silica. Distillate solution was tap water. Inlet temperatures of feed and distillation were 50ºC and 20 ºC, respectively. Crossflow rate for feed and distillate was 600 mL/min co-currently.

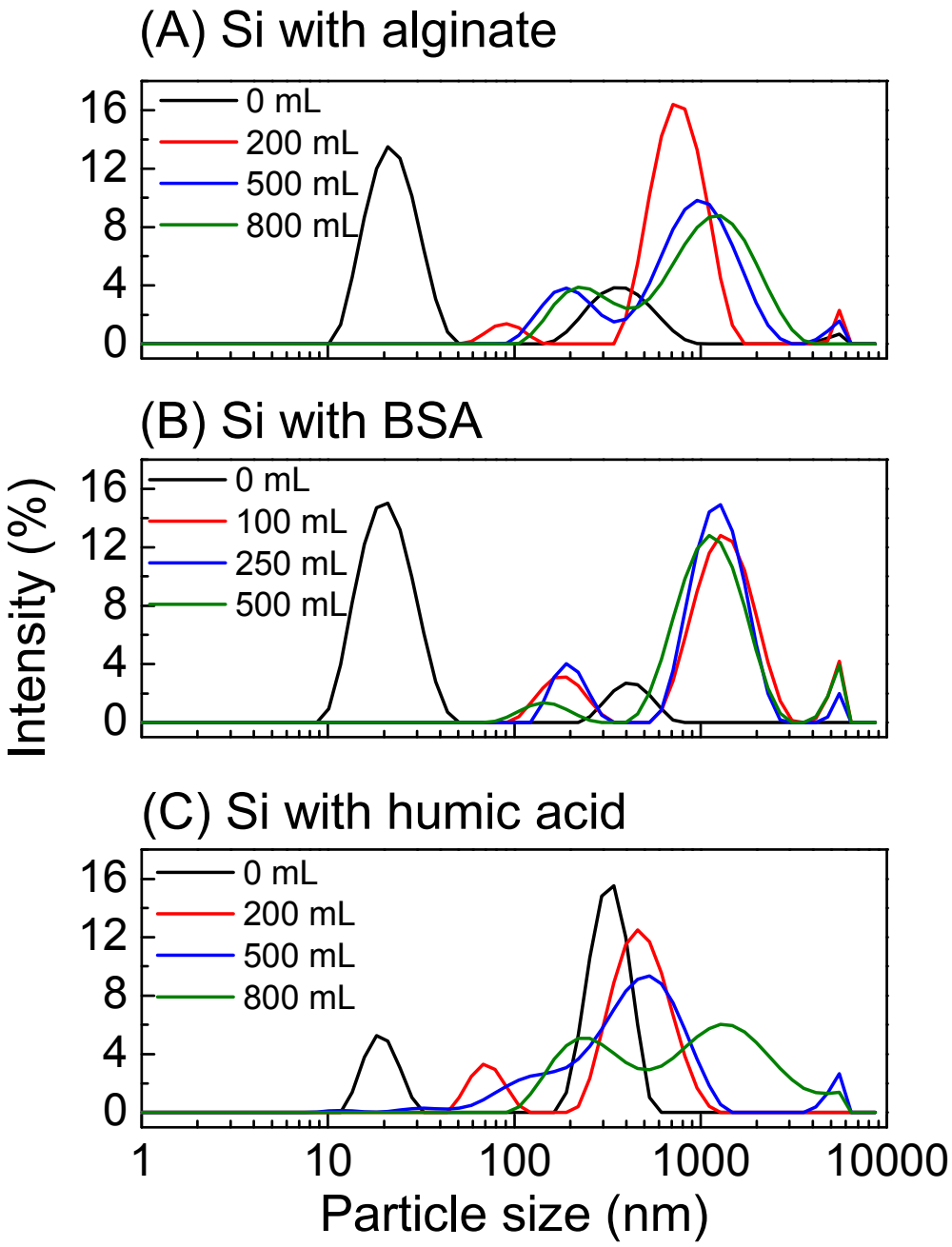

473

474 **Figure 5:** Feed solution particle size as a function of cumulative permeate volume during
475 combined fouling in membrane distillation: (A) colloidal silica with alginate, (B) colloidal
476 silica with BSA, and (C) colloidal silica with humic acid. Experimental conditions were
477 described in figures 2-4.

478

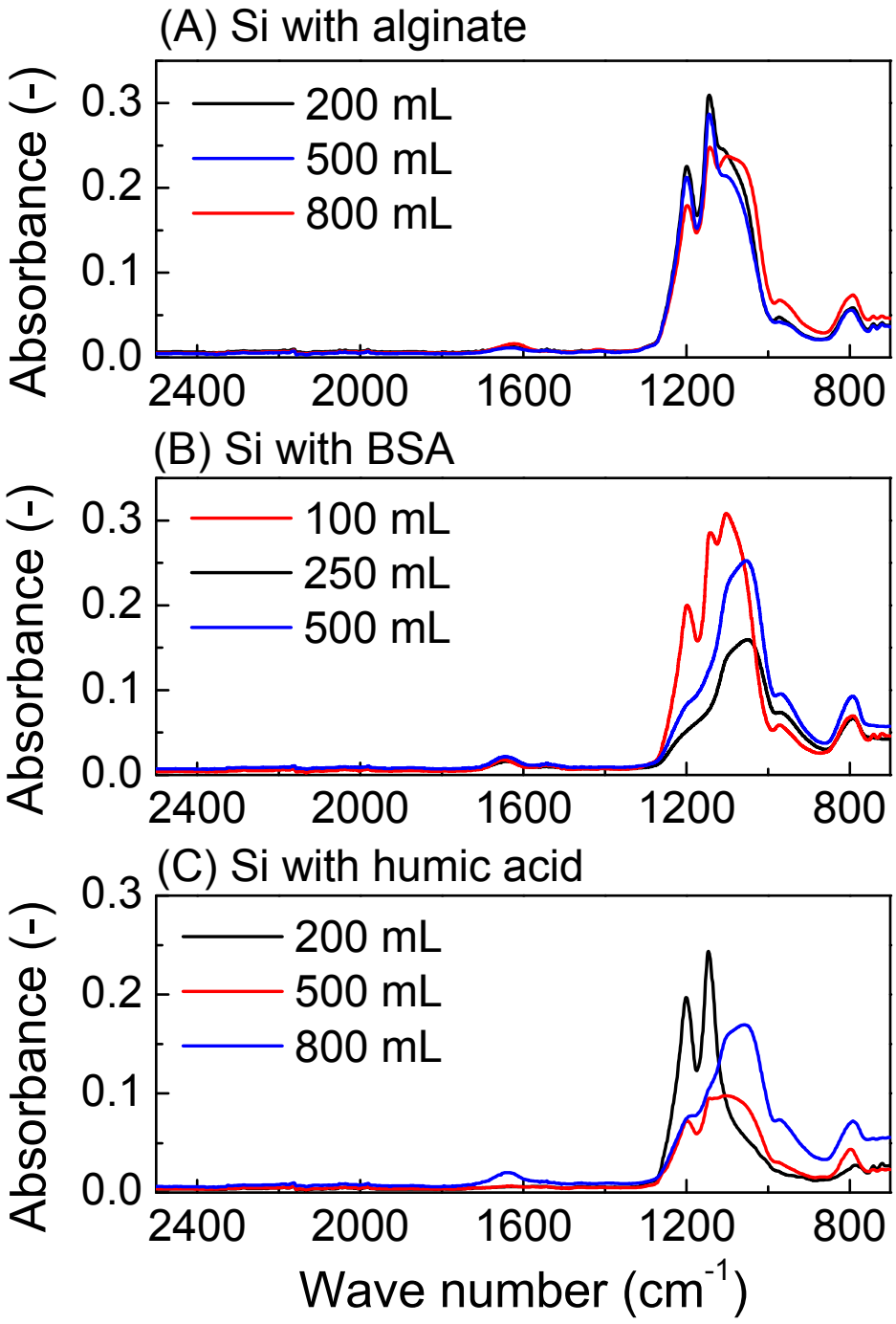

479

480 **Figure 6:** Fourier transform infrared spectra as a function of cumulative permeate volume of
481 fouled membrane in membrane distillation by (A) colloidal silica with alginate, (B) colloidal
482 silica with BSA, and (C) colloidal silica with humic acid. Experimental conditions were
483 described in figures 2-4.

484

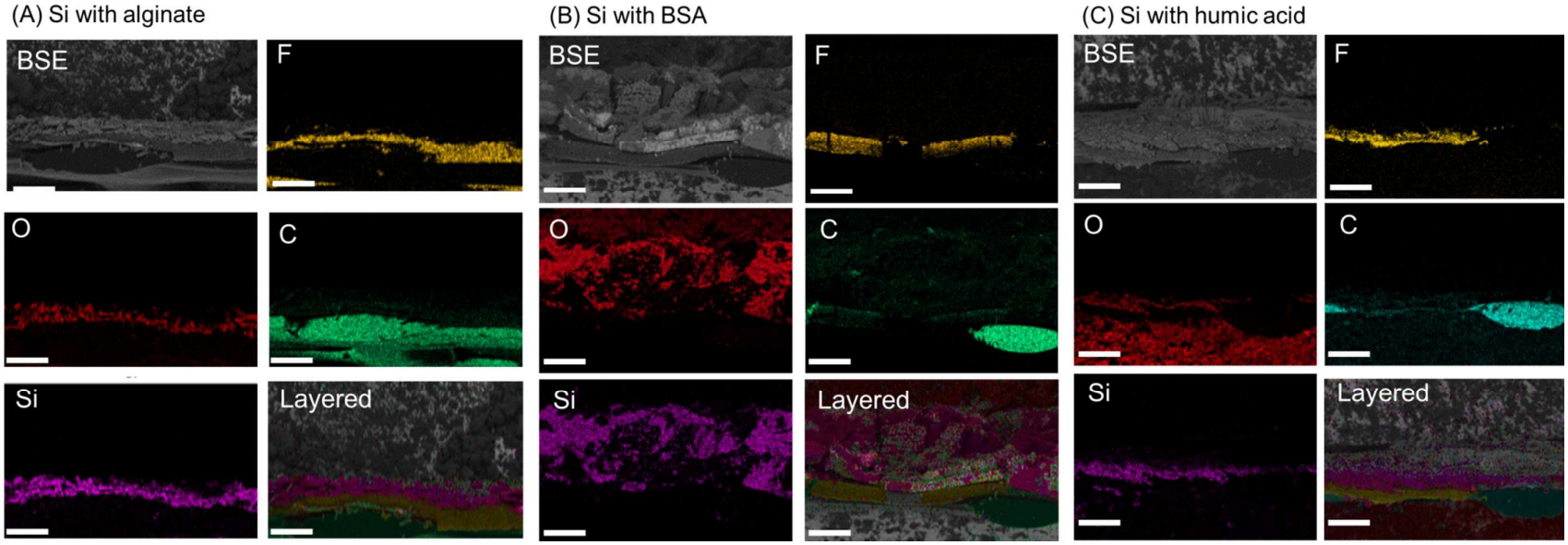

Figure 7: Element mapping by Energy-dispersive X-ray spectroscopy of fouled membrane in membrane distillation by (A) colloidal silica with alginate, (B) colloidal silica with BSA, and (C) colloidal silica with humic acid, at the conclusion of experiment. Experimental conditions were described in figures 2-4. The back scattering electron (BSE) image was used for element mapping, and the distribution and relative location of key elements were presented in the layered image. Scale bar corresponds to 100 μm.

Graphical abstract image